



# Bandgap engineering of $(\text{AgIn})_x\text{Zn}_{2(1-x)}\text{S}_2$ quantum dot photosensitizers for photocatalytic $\text{H}_2$ generation

Yong-Jun Yuan <sup>a,\*</sup>, Da-Qin Chen <sup>a,\*</sup>, Mian Xiong <sup>a</sup>, Jia-Song Zhong <sup>a</sup>, Zhong-Yi Wan <sup>a</sup>, Yang Zhou <sup>a</sup>, Shen Liu <sup>a</sup>, Zhen-Tao Yu <sup>b,\*</sup>, Ling-Xia Yang <sup>b</sup>, Zhi-Gang Zou <sup>b</sup>

<sup>a</sup> College of Materials and Environmental Engineering, Hangzhou Dianzi University, Hangzhou 310018, People's Republic of China

<sup>b</sup> National Laboratory of Solid State Microstructures and Collaborative Innovation Center of Advanced Microstructures, Jiangsu Key Laboratory for Nano Technology, College of Engineering and Applied Science, Nanjing University, Nanjing 210093, People's Republic of China

## ARTICLE INFO

### Article history:

Received 23 September 2016

Received in revised form 2 November 2016

Accepted 13 November 2016

Available online 15 November 2016

## ABSTRACT

Semiconductor quantum dots are extremely interesting photosensitizers for the development of solar hydrogen generation. However, most efficient quantum dots prepared with toxic heavy metal of Cd were limited by high toxicity and poor absorbance in visible and near-infrared regions. Herein we achieve effective composition regulation of  $(\text{AgIn})_x\text{Zn}_{2(1-x)}\text{S}_2$  that provides bandgap-tunable quantum dots, leading to the development of high efficiency quantum dots photosensitizer with low toxicity for solar  $\text{H}_2$  generation in a three-component system in combination with a molecular cobalt catalyst and ascorbic acid as the sacrificial reagent. The composition of  $(\text{AgIn})_x\text{Zn}_{2(1-x)}\text{S}_2$  quantum dots can be continuously tuned from  $x=0$  ( $\text{ZnS}$ ) at one end to  $x=1$  ( $\text{AgInS}_2$ ) at the other end, resulting in the corresponding bandgap being modulated gradually from 3.55 eV to 1.80 eV. The effect of bandgap on photocatalytic performance of  $(\text{AgIn})_x\text{Zn}_{2(1-x)}\text{S}_2$  quantum dots was investigated, and the results show that a balance between the light absorption capacity and the driving force decided by the bandgap in the  $(\text{AgIn})_{0.5}\text{ZnS}_2$  quantum dots leads to the highest efficiency of visible light driven  $\text{H}_2$  generation. A high apparent quantum yield of 8.2% under monochromatic irradiation at 450 nm is obtained for this photocatalytic system. This efficiency is the best performance to date for solar  $\text{H}_2$  generation system based on Cd-free quantum dots. It is believed that this bandgap-tunable  $(\text{AgIn})_x\text{Zn}_{2(1-x)}\text{S}_2$  quantum dots would have great potential as durable and lowly toxic photosensitizers to replace commonly-used Cd-based and molecular dyes for highly-efficient solar  $\text{H}_2$  generation.

© 2016 Elsevier B.V. All rights reserved.

## 1. Introduction

Solar  $\text{H}_2$  generation from water through artificial photosynthesis represents a sustainable and carbon-free approach to process the increasingly serious energy crisis and environmental pollution problems [1–4]. Constructing an efficient photocatalytic water splitting system has been a major focus of research toward solar  $\text{H}_2$  generation. During the photocatalytic  $\text{H}_2$  generation processes, the photons were absorbed by the light absorber to trigger photocatalytic reduction of water into valuable  $\text{H}_2$ , and the light trapping capability of the light absorber is a key component in determining the overall solar-to- $\text{H}_2$  conversion efficient. So far, various semiconductors and molecular dyes have been extensively investigated as

light absorbers in heterogeneous or homogeneous photocatalytic  $\text{H}_2$  production systems [5–10]. However, these photocatalytic  $\text{H}_2$  production system typical employ light absorbers that are either toxic ( $\text{CdS}$ ,  $\text{CdSe}$ ) [11,12], expensive (ruthenium, iridium and platinum complex dyes) [13–17], unstable (organic dyes) [18,19], or inactive under visible light illumination ( $\text{TiO}_2$  and  $\text{ZnO}$ ) [20,21], which limit their practical application for solar  $\text{H}_2$  generation.

More recently, semiconductor quantum dots (QDs) are regarded as excellent light-harvesting photosensitizers for solar  $\text{H}_2$  production owing to their favorable advantages including large extinction coefficients, multiple exciton generation, readily modifiable surfaces and enhanced photostability [22–25]. Unlike to bulk semiconductors with fast trap-mediated electron-hole recombination, the QDs exhibit large surface-to-volume ratios and quantum confinement, which should lead to enhanced surface amplitude of charge carriers for  $\text{H}_2$  generation. Compared to molecular dyes, the size-dependent optical properties and large extinction coefficients of QDs significantly improve the light-harvesting performance.

\* Corresponding authors.

E-mail addresses: [yjyuan@hdu.edu.cn](mailto:yjyuan@hdu.edu.cn) (Y.-J. Yuan), [dqchen@hdu.edu.cn](mailto:dqchen@hdu.edu.cn) (D.-Q. Chen), [yuzt@nju.edu.cn](mailto:yuzt@nju.edu.cn) (Z.-T. Yu).

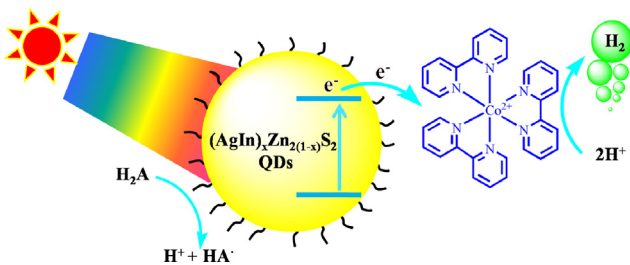


**Fig. 1.** Schematic representation of three-component photocatalytic H<sub>2</sub> production system comprising (AgIn)<sub>x</sub>Zn<sub>2(1-x)</sub>S<sub>2</sub> QDs as photosensitizers, [Co(bpy)<sub>3</sub>]<sup>2+</sup> as the catalyst and H<sub>2</sub>A as the sacrificial electron donor.

Especially for binary Cd-based semiconductor QDs, such as CdS [26–28], CdSe [29–32] and CdTd [33–36], which have been intensively investigated as highly-efficient photosensitizers for solar H<sub>2</sub> generation in semi-heterogeneous colloidal photocatalytic H<sub>2</sub> production systems in conjunction with a water reduction catalyst. For example, Esienberg's group reported visible-light-driven H<sub>2</sub> production systems typically consist of CdSe QDs, a molecular nickel catalyst and ascorbic acid, which showed the highest hydrogen production efficiency for water-reduction catalysis in a three-component system reported to date [37]. Despite some significant process has been made in photocatalytic H<sub>2</sub> production systems based on Cd-based QDs, but the practical application of Cd-based QDs photosensitizers is limited by the high toxicity of cadmium. Furthermore, the bandgap of Cd-based QDs cannot be efficiently tuned to absorb red and near-infrared light, which makes these Cd-based quantum dots to be inactive photosensitizers under red or near-infrared light irradiation. From the point of view of capturing more sunlight, tuning the bandgap of QDs is a great challenge in field of solar-to-H<sub>2</sub> conversion. Therefore, it is highly desirable to develop bandgap-tunable Cd-free QDs photosensitizers for solar H<sub>2</sub> generation.

In this study, bandgaps of (AgIn)<sub>x</sub>Zn<sub>2(1-x)</sub>S<sub>2</sub> solid solution quantum dots are engineered by controlling their chemical composition, the tunable bandgaps of (AgIn)<sub>x</sub>Zn<sub>2(1-x)</sub>S<sub>2</sub> QDs are attractive feature for solar H<sub>2</sub> generation because they exhibit a wide wavelength range of absorption from ultraviolet to visible and near-infrared regions. The relation between bandgap and photocatalytic performance of (AgIn)<sub>x</sub>Zn<sub>2(1-x)</sub>S<sub>2</sub> QDs were studied in heterogeneous photocatalytic H<sub>2</sub> production systems in combination with [Co(bpy)<sub>3</sub>]<sup>2+</sup> (bpy = 2,2'-bipyridine) catalyst and ascorbic acid (H<sub>2</sub>A) as a sacrificial reagent (Fig. 1). The synthesized (AgIn)<sub>x</sub>Zn<sub>2(1-x)</sub>S<sub>2</sub> QDs with long excited-state lifetimes, promising light-harvesting property as well as their low-toxicity, which were regarded as the most suitable alternative to Cd-based semiconductor QDs for solar-to-H<sub>2</sub> conversion.

## 2. Experiment section

### 2.1. General procedures

Commercially available chemical reagents were used without purification. [Ir(ppy)<sub>2</sub>bpy](PF<sub>6</sub>) [38], Ru[(bpy)<sub>3</sub>](PF<sub>6</sub>)<sub>2</sub> [39], were prepared according to literature procedures. The structural study of as-prepared (AgIn)<sub>x</sub>Zn<sub>2(1-x)</sub>S<sub>2</sub> QDs was performed using X-ray diffractometer (XRD, Bruker D8) with Cu K $\alpha$  irradiation ( $\lambda = 0.15406$  nm). UV-vis absorption spectra and photoluminescence (PL) spectra of (AgIn)<sub>x</sub>Zn<sub>2(1-x)</sub>S<sub>2</sub> QDs solutions were analyzed in a 1 cm path length quartz cell on an Edinburgh FS5 spectrophotofluorometer equipped with an 150 W Xenon as the excitation source. The morphological study of the samples was obtained using transmission electron microscopy (TEM, JEM 2010, JEOL) with an accelerating voltage of 200 kV, and all the samples were pre-

pared by depositing a drop of diluted suspensions in ethanol on a carbon-film-coated copper grid and naturally dried. The surface characterizations of (AgIn)<sub>x</sub>Zn<sub>2(1-x)</sub>S<sub>2</sub> QDs were performed using X-ray Photoelectron spectroscopy (XPS, VG ESCALAB MKII) with Mg Al K $\alpha$  X-ray source and a charge neutralizer. All the binding energies were corrected by using the C1s peak at 284.8 eV. Fourier transform infrared spectrometer (FT-IR) of the samples was carried out on a Nicolet 5700 FT-IR spectrometer in the wavenumber range from 400 to 4000 cm<sup>-1</sup> by using the conventional KBr pellets. The time-resolved PL spectra were measured on an Edinburgh LifeSpec II spectrophotofluorometer equipped with a 465 nm picosecond laser as the excitation source.

### 2.2. Synthesis of (AgIn)<sub>x</sub>Zn<sub>2(1-x)</sub>S<sub>2</sub> quantum dots

(AgIn)<sub>x</sub>Zn<sub>2(1-x)</sub>S<sub>2</sub> QDs were prepared through thermal reaction of metal acetate and thiourea in a 9:1 oleylamine/1-dodecanthiol solution similar to that reported by Torimoto et al. [40]. Powders of Ag(CH<sub>3</sub>COO)<sub>x</sub>, In(CH<sub>3</sub>COO)<sub>3</sub>, and Zn(CH<sub>3</sub>COO)<sub>2</sub>·2H<sub>2</sub>O with a mole ratio of x/x/2(1-x) (total metal ions: 1 mmol) were mixed with 27 mL of oleylamine and 3 mL of 1-dodecanthiol in a 100 mL three-neck-flask under a N<sub>2</sub> atmosphere. After these metal acetate precursors were dissolved completely, 76 mg thiourea (1 mmol) was added into the mixture solution. Then, the reaction solution was heated at 250 °C for 15 min under magnetic stirring. The color of solution was changed to dark. After the solution was cooled naturally to room temperature, the large aggregated particles were removed from the solution by centrifugation. The (AgIn)<sub>x</sub>Zn<sub>2(1-x)</sub>S<sub>2</sub> QDs were isolated from the supernatant by precipitation with the addition of ethanol. The produced powder was separated by high-speed centrifugation, followed by washing with ethanol for five times and drying in a vacuum oven at 60 °C for 12 h.

### 2.3. Synthesis of [Co(bpy)<sub>3</sub>]<sup>2+</sup> catalyst

[Co(bpy)<sub>3</sub>]<sup>2+</sup> catalyst was synthesized by adding 3.2 equiv of 2,2'-bipyridine ligand to the cobalt chloride hexahydrate according to our previously report [38]. Typically, 2,2'-bipyridine (2.12 g, 14.0 mmol) and cobalt chloride hexahydrate (0.95 g, 4.0 mmol) were added to absolute ethanol (50 mL), and the reaction was heated at 80 °C for 12 h. After the mixture was cooled and concentrated to 10 mL volume by rotary evaporation, 20 mL of diethyl ether was added into the round-bottomed flask; the resulting red precipitate was isolated by filtration and dried under vacuum. The crude product was recrystallized by acetone/n-hexane vapor diffusion, giving the pure [Co(bpy)<sub>3</sub>]<sup>2+</sup> as a red crystalline solid in 78% yield. IR (KBr):  $\nu = 3072$  ( $\nu_{\text{s}}(\text{C-H})$ ), 1600 ( $\nu_{\text{s}}(\text{C=C})$ ), 1317 ( $\nu_{\text{s}}(\text{C-N})$ ), 1017 ( $\nu_{\text{s}}(\text{C-C})$ ), 779 cm<sup>-1</sup> ( $\nu_{\text{g}}(\text{C-H})$ ); Anal. Calcd. for C<sub>20</sub>H<sub>16</sub>N<sub>4</sub>Cl<sub>2</sub>Co: C 54.23, H 3.57, N 8.2; Found: C 54.09, H 3.71, N 12.44.

### 2.4. Photocatalytic hydrogen production

While these experiments were carried out, best practices in heterogeneous photocatalytic H<sub>2</sub> evolution measurements were followed [41]. Photocatalytic H<sub>2</sub> production reactions were carried out in an outer irradiation-type Pyrex glass cell with a top window connected to a closed gas-circulation system. In a typical photocatalytic hydrogen production experiment, samples in toluene-ethanol-water solution (100 mL, 6:3:1) containing of 10  $\mu$ M QDs photosensitizer, 1 mM [Co(bpy)<sub>3</sub>]<sup>2+</sup> catalyst and 0.1 M H<sub>2</sub>A were prepared in a 150 mL glass cell. After the air was removed completely, the reactant solution was irradiated by a 300 W Xe lamp (SEX 200, Shengyang Yirida Co. Ltd, China) equipped with a cutoff filter ( $\lambda > 420$  nm). The reaction temperature of solution was maintained at room temperature by a flow of cooling water during

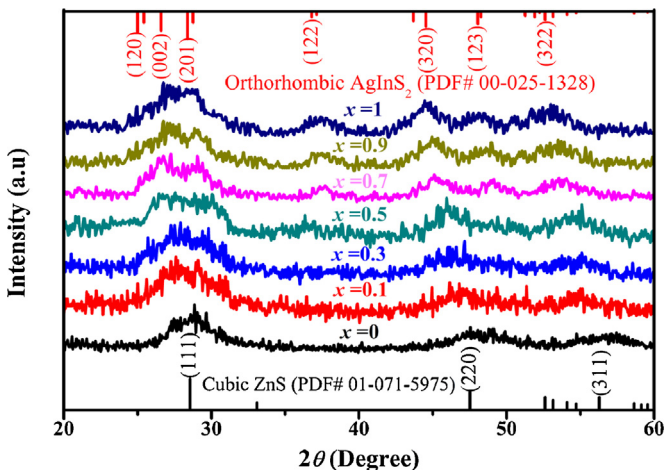


**Fig. 2.** XRD patterns of ZnS, AgInS<sub>2</sub> and (AgIn)<sub>x</sub>Zn<sub>2(1-x)</sub>S<sub>2</sub> QDs with different x values of 0.1, 0.3, 0.5, 0.7 and 0.9. XRD patterns of bulk materials are also shown for cubic ZnS (JCPDS No. 01-071-5975) and orthorhombic AgInS<sub>2</sub> (JCPDS No. 00-025-1328).

the H<sub>2</sub> production reaction. The amount of H<sub>2</sub> produced was determined by using an on-line gas chromatograph (GC, JieDuo-609, MS-5 Å molecular sieve columns, TCD detector, Argon carrier). The apparent quantum yield (AQY) was measured under the same photocatalytic reaction except for irradiation light provided by a low blue LED (1 W, 450 nm) (Shenzhen Warner JPLED Co. Ltd. China). The AQY was calculated by the following equations [2]:

$$\text{AQY}[\%] = \frac{\text{number of reacted electrons}}{\text{number of incident protons}} \times 100$$

$$= \frac{2 \times \text{number of evolved H}_2 \text{ molecules}}{\text{number of incident protons}} \times 100$$

### 3. Results and discussion

#### 3.1. Characterization of (AgIn)<sub>x</sub>Zn<sub>2(1-x)</sub>S<sub>2</sub> QDs

The (AgIn)<sub>x</sub>Zn<sub>2(1-x)</sub>S<sub>2</sub> solid solution QDs with different Zn/Ag ratios were synthesized through a facile solvent-thermal reaction method from Zn(CH<sub>3</sub>COO)<sub>2</sub>, In(CH<sub>3</sub>COO)<sub>3</sub>, Ag(CH<sub>3</sub>COO) and thiourea using a mixed solvent of 1-dodecanethiol and oleylamine in a 1:9 ratio. The synthesized (AgIn)<sub>x</sub>Zn<sub>2(1-x)</sub>S<sub>2</sub> QDs are very soluble in many organic nonpolar solvents such as n-hexane, dichloromethane and toluene, and their colloidal solutions are stable for over six months when stored at room temperature. Fourier transform infrared spectroscopy (FT-IR) measurement revealed number of weak peaks between  $\nu$ 1400–1650 cm<sup>-1</sup> and  $\nu$ 2800–3000 cm<sup>-1</sup>, which can be assigned to the symmetric and asymmetric stretching of the –CH<sub>2</sub> groups, terminal –CH<sub>3</sub> and =C–H of oleylamine (Fig. S1 in Supporting information), indicating that oleylamine molecules were attached on the surface of (AgIn)<sub>x</sub>Zn<sub>2(1-x)</sub>S<sub>2</sub> QDs [42].

The obtained QDs were then subject to X-ray diffraction (XRD) measurement to verify their crystal structure. XRD patterns of pure ZnS, AgInS<sub>2</sub> and (AgIn)<sub>x</sub>Zn<sub>2(1-x)</sub>S<sub>2</sub> QDs were compared in Fig. 2, where distinguishable difference in reflection peak angle was observed. All samples show very broad peaks due to their small particle sizes, and the crystal structure depended on their chemical composition. Seven major peaks of pure AgInS<sub>2</sub> QDs appeared at almost the same diffraction angles as those for the orthorhombic crystal structure of bulk AgInS<sub>2</sub> (JCPDS No. 00-025-1328) and were assignable to (120), (002), (201), (122), (320), (123), and (322) planes, respectively. In contrast, three broad peaks were observed at 28.7, 47.5, and 56.4° for pure ZnS QDs, which can be

assigned to (111), (220), and (311) planes of cubic ZnS (JCPDS No. 01-071-5975), respectively [43]. As shown in the XRD patterns of as-prepared (AgIn)<sub>x</sub>Zn<sub>2(1-x)</sub>S<sub>2</sub> QDs, the (AgIn)<sub>x</sub>Zn<sub>2(1-x)</sub>S<sub>2</sub> QDs with x > 0.5 exhibited diffraction patterns similar to those for pure AgInS<sub>2</sub> QDs. In contrast, three broad peaks appeared at almost the same diffraction angles as those for the pure ZnS QDs were observed for (AgIn)<sub>x</sub>Zn<sub>2(1-x)</sub>S<sub>2</sub> QDs samples with x < 0.5. It is clear that the diffraction peaks were shifted to lower angles with an increase in the x values, indicating that the synthesized QDs were not mixtures of AgInS<sub>2</sub> and ZnS nanoparticles but were composed of solid solution between AgInS<sub>2</sub> and ZnS [43,44].

The shape, size and nature of (AgIn)<sub>x</sub>Zn<sub>2(1-x)</sub>S<sub>2</sub> QDs were investigated by TEM. As shown in Fig. 3a and b, the typical TEM images of representative (AgIn)<sub>0.3</sub>Zn<sub>1.4</sub>S<sub>2</sub> QDs prepared in 1-dodecanethiol/oleylamine mixture solution containing 20 mM metal acetate precursors showed that the (AgIn)<sub>0.3</sub>Zn<sub>1.4</sub>S<sub>2</sub> QDs were made up of spherical nanoparticles with diameters from 2.3 to 4.1 nm (Fig. S2), and the average diameter of the (AgIn)<sub>0.3</sub>Zn<sub>1.4</sub>S<sub>2</sub> QDs was determined to be about 3.4 nm. It is noticeable that the size of (AgIn)<sub>0.3</sub>Zn<sub>1.4</sub>S<sub>2</sub> QDs could also be controlled by changing the concentration of metal acetate precursors. Figs. S3 and S4 showed typical TEM images of (AgIn)<sub>0.3</sub>Zn<sub>1.4</sub>S<sub>2</sub> QDs prepared in 1-dodecanethiol/oleylamine mixture solution containing 10 and 60 mM metal acetate precursors, whose size was estimated to be 2.1 and 4.4 nm, respectively. Consequently, we concluded that the particle size of (AgIn)<sub>0.3</sub>Zn<sub>1.4</sub>S<sub>2</sub> QDs increased with the concentration of metal acetate precursors used in the reaction solution, the present synthetic strategy enables independent control of the particle size of (AgIn)<sub>0.3</sub>Zn<sub>1.4</sub>S<sub>2</sub> QDs. Although the particle size of the (AgIn)<sub>0.3</sub>Zn<sub>1.4</sub>S<sub>2</sub> QDs is small, well-resolved lattice fringes are observed in the high-resolution TEM (HRTEM) image illustrated in Fig. 3c, indicating high crystallinity of (AgIn)<sub>0.3</sub>Zn<sub>1.4</sub>S<sub>2</sub> QDs. As shown in Fig. 3d, the lattice spacing were measured to be 0.23 and 0.33 nm, corresponding to the (102) planes of AgInS<sub>2</sub> and (100) planes ZnS exhibited in the (AgIn)<sub>0.3</sub>Zn<sub>1.4</sub>S<sub>2</sub> QDs, respectively [45]. As shown in Fig. 3e and f, the (AgIn)<sub>0.5</sub>ZnS<sub>2</sub> QDs sample exhibited at almost the same size as that of the (AgIn)<sub>0.3</sub>Zn<sub>1.4</sub>S<sub>2</sub> QDs, the average diameter of the (AgIn)<sub>0.5</sub>ZnS<sub>2</sub> QDs was measured to be about 3.5 nm (Fig. S5).

X-ray photoelectron spectroscopy (XPS) analysis was used to examine the chemical states of (AgIn)<sub>x</sub>Zn<sub>2(1-x)</sub>S QDs. As shown in Fig. 4a, the wide-scan XPS spectra of (AgIn)<sub>0.3</sub>Zn<sub>1.4</sub>S<sub>2</sub> QDs presented strong Zn 2p, In 3d, Ag 3d, and S 2s bands at 1022.3, 444.8, 366.4 and 161.9 eV, respectively. More importantly, the Zn/Ag/In atomic ratio was found to be ~3:3:14, which is in good agreement with the nominal chemical composition of (AgIn)<sub>0.3</sub>Zn<sub>1.4</sub>S<sub>2</sub> QDs. In the high-resolution XPS spectrum of Zn 2p illustrated in Fig. 4b, two peaks at 1021.3 and 1044.3 eV appear, indicative of Zn<sup>2+</sup> with a splitting of 23.0 eV, which is very close to the standard separation of 22.9 eV. The Ag 3d peaks located at 368.4 and 374.3 eV, and a peak splitting of 5.9 eV indicates Ag<sup>+</sup> (Fig. 4c). The In<sup>3+</sup> is confirmed by a peak splitting of 7.5 eV of two peaks located at 444.8 and 452.3 eV, respectively (Fig. 4d). Two S2p peaks are located at 161.8 and 163.1 eV, respectively, showing a peak separation of 1.3 eV (Fig. 4e). As shown in Fig. 4f, the Zn2p peaks, Zn2p<sub>3/2</sub> and Zn2p<sub>1/2</sub>, appear at 1020.9 and 1043.8 eV in bare ZnS QDs, are different with those of (AgIn)<sub>0.3</sub>Zn<sub>1.4</sub>S<sub>2</sub> at 1021.3 and 1044.3 eV, indicating that the chemical circumstance of Zn in (AgIn)<sub>0.3</sub>Zn<sub>1.4</sub>S<sub>2</sub> is different from that in pure ZnS. The higher binding energy shift of Zn2p in (AgIn)<sub>0.3</sub>Zn<sub>1.4</sub>S<sub>2</sub> QDs could be attributed to the strong interaction between ZnS and AgInS<sub>2</sub> components.

Fig. 5a shows the absorption spectra of ZnS, AgInS<sub>2</sub> and (AgIn)<sub>x</sub>Zn<sub>2(1-x)</sub>S<sub>2</sub> QDs. The bare ZnS QDs with a wide bandgap ( $E_{bg}$  = 3.55 eV) has an ultraviolet light absorption band. In contrast, the (AgIn)<sub>x</sub>Zn<sub>2(1-x)</sub>S<sub>2</sub> QDs have strong absorption bands in visible light region even with a tail in near-infrared region. The

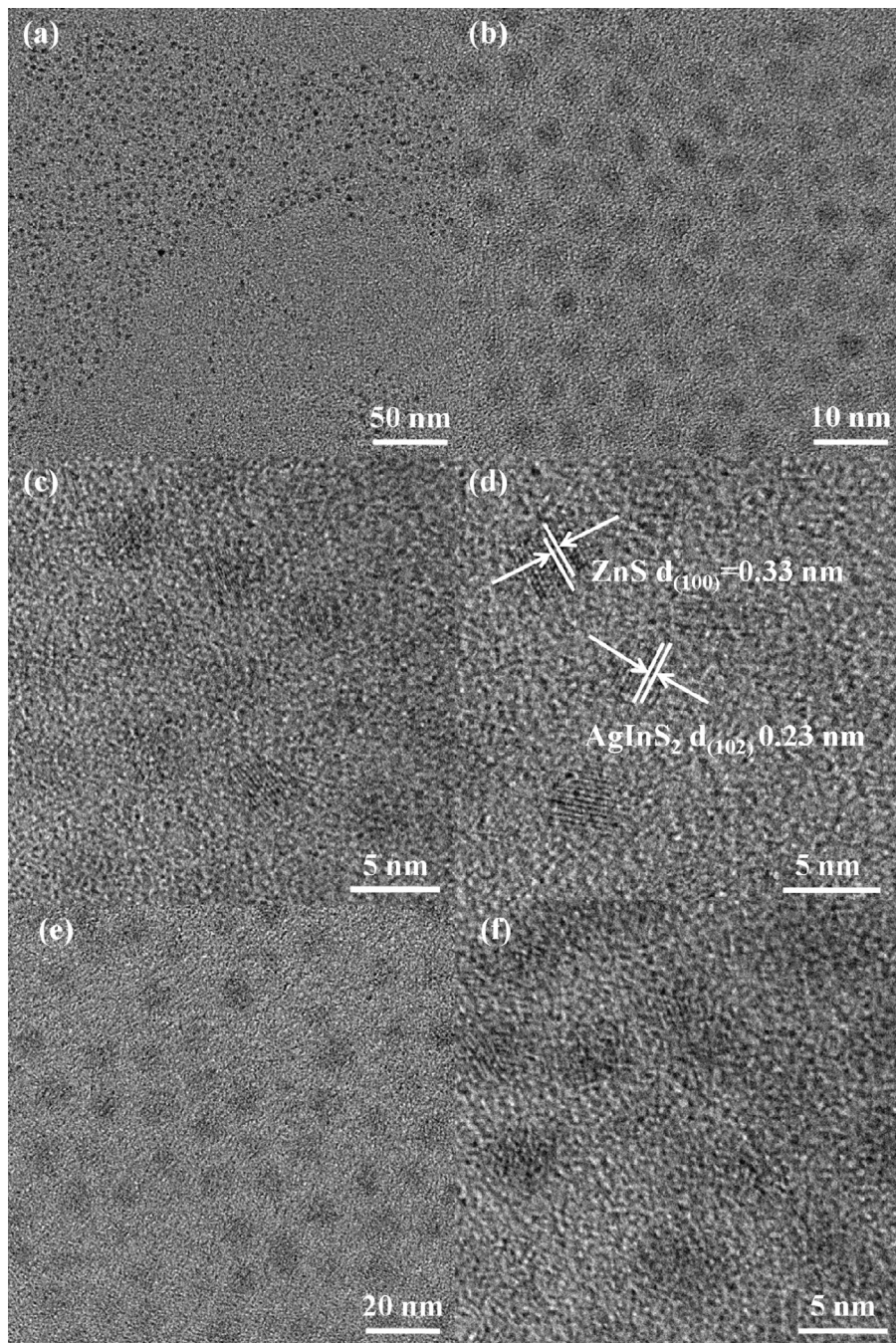


**Fig. 3.** TEM (a, b) and HRTEM (c, d) images of  $(\text{AgIn})_{0.3}\text{Zn}_{1.4}\text{S}_2$  QDs; HRTEM (e,f) images of  $(\text{AgIn})_{0.5}\text{ZnS}_2$  QDs.

steep shapes of the visible edges reveal that the absorption band of  $(\text{AgIn})_x\text{Zn}_{2(1-x)}\text{S}_2$  QDs was due to the transition from the valence band (VB) to the conduction band (CB). On the other hand, all  $(\text{AgIn})_x\text{Zn}_{2(1-x)}\text{S}_2$  QDs samples show strong luminescence in the visible and near-infrared region illustrated in Fig. 5b. It is noticeable that a red- shift in both absorption and emission maxima was observed as the ratio of  $\text{AgInS}_2$  to  $\text{ZnS}$  increased, which could be attributed to the decreasing bandgaps resulted from the interaction of energy bands (Fig. S6) [44]. The bandgaps of  $(\text{AgIn})_x\text{Zn}_{2(1-x)}\text{S}_2$  QDs with different  $x$  values of 0.1, 0.3, 0.5, 0.7 and 0.9 estimated from the intersection of the normalized absorption and emission spectra (Fig. S6) [46], which was calculated to be 2.78, 2.56, 2.34, 2.21 and 2.02 eV, respectively. The decreased bandgaps are well consistent with the colors of the  $(\text{AgIn})_x\text{Zn}_{2(1-x)}\text{S}_2$  QDs in  $\text{CH}_2\text{Cl}_2$

solutions change from colorless to dark red as the ratio of  $\text{AgInS}_2$  to  $\text{ZnS}$  was increased (Fig. 5c). Taking into account the efficiency using of visible light in a large part of the solar spectrum, we believe that these  $(\text{AgIn})_x\text{Zn}_{2(1-x)}\text{S}_2$  QDs samples with their strong absorption in the visible region, are attractive photosensitizers for solar-to- $\text{H}_2$  conversion. Excited lifetimes of  $(\text{AgIn})_x\text{Zn}_{2(1-x)}\text{S}_2$  QDs were then investigated by time-resolved PL spectroscopy. As shown in Fig. 5d, the synthesized  $(\text{AgIn})_x\text{Zn}_{2(1-x)}\text{S}_2$  QDs exhibited excited state lifetimes in the range of 0.36 to 0.53  $\mu\text{s}$ , which are longer than those of previously reported  $\text{CdS}$  [47],  $\text{CdSe}$  [48],  $\text{CdTe}$  QDs [38] in ns timescale. The long excited lifetimes of  $(\text{AgIn})_x\text{Zn}_{2(1-x)}\text{S}_2$  QDs are very important for charge carrier transfer, which would make these  $(\text{AgIn})_x\text{Zn}_{2(1-x)}\text{S}_2$  QDs to be attractive photosensitizers for photoinduced electron transfer reactions.

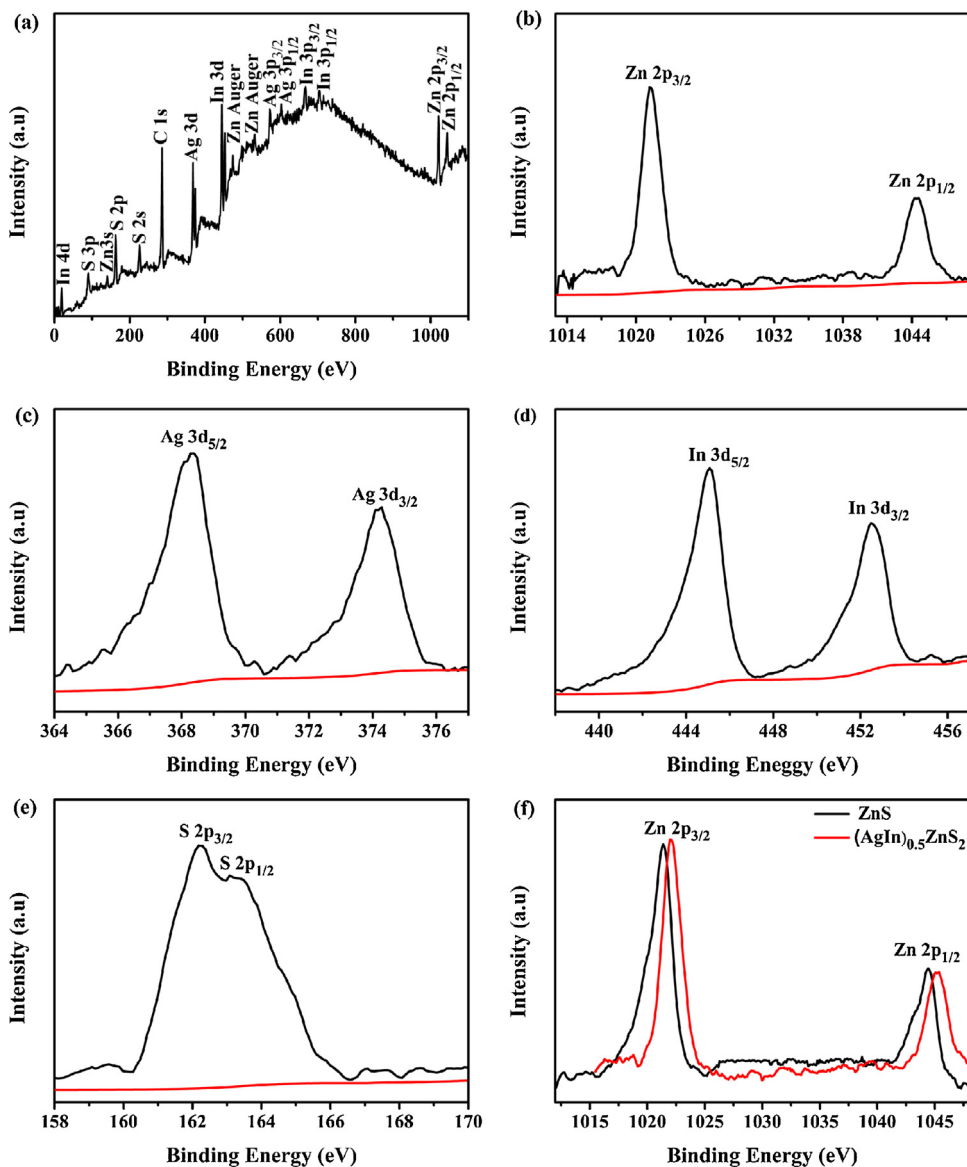


**Fig. 4.** (a) Wide-scan XPS spectrum of  $(\text{AgIn})_x\text{Zn}_{1.4}\text{S}_2$  QDs; high-resolution XPS spectra of Zn 2p (b), Ag 3d (c), In 3d (d) and S2p (e) in  $(\text{AgIn})_x\text{Zn}_{1.4}\text{S}_2$  QDs; (f) high-resolution XPS spectrum of Zn 2p in pure ZnS and  $(\text{AgIn})_x\text{Zn}_{1.4}\text{S}_2$  samples.

### 3.2. Photocatalytic activities of $(\text{AgIn})_x\text{Zn}_{2(1-x)}\text{S}_2$ QDs

Based on those above-mentioned excellent photophysics properties including tunable visible light absorption and long excited state lifetimes, the synthesized  $(\text{AgIn})_x\text{Zn}_{2(1-x)}\text{S}_2$  QDs would be appropriate photosensitizers for photocatalytic H<sub>2</sub> generation. To investigate the photocatalytic performance of  $(\text{AgIn})_x\text{Zn}_{2(1-x)}\text{S}_2$  QDs, an initial photocatalytic H<sub>2</sub> production experiment of  $(\text{AgIn})_x\text{Zn}_{2(1-x)}\text{S}_2$  QDs with [Co(bpy)<sub>3</sub>]<sup>2+</sup> catalyst was evaluated in the presence of

H<sub>2</sub>A as a sacrificial electron donor. To keep the solubility of  $(\text{AgIn})_x\text{Zn}_{2(1-x)}\text{S}_2$  QDs through-out the experiment, we carried out the photocatalytic reaction in 6:3:1 toluene-ethanol-water solution. In typically experiment, 100 ml of anaerobic solution containing 10  $\mu\text{M}$   $(\text{AgIn})_x\text{Zn}_{2(1-x)}\text{S}_2$  QDs, 1 mM [Co(bpy)<sub>3</sub>]<sup>2+</sup> and 100 mM H<sub>2</sub>A was irradiated by a 300 W Xe lamp with a cutoff filter ( $\lambda > 420 \text{ nm}$ ) at room temperature. The headspace H<sub>2</sub> gas was characterized by gas chromatography (GC) analysis. Control experiments in the absence of either  $(\text{AgIn})_x\text{Zn}_{2(1-x)}\text{S}_2$  QDs or light irradiation produced no appreciable amount of H<sub>2</sub>, indicating the  $(\text{AgIn})_x\text{Zn}_{2(1-x)}\text{S}_2$  QDs was essential and the H<sub>2</sub> production pro-

cess is a light catalyzed reaction. On the other hand, visible light irradiation of  $(\text{AgIn})_x\text{Zn}_{2(1-x)}\text{S}_2$  QDs in the absence of H<sub>2</sub>A do not allow the detection of any hydrogen, indicating that the H<sub>2</sub>A was an essential component for H<sub>2</sub> production. That is, the H<sub>2</sub>A acted as a sacrificial electron donor can scavenge the holes and reduce the charge carrier recombination, resulting in significantly improved photocatalytic H<sub>2</sub> evolution activity.

Fig. 6a shows the effect of chemical composition on the photocatalytic performance of  $(\text{AgIn})_x\text{Zn}_{2(1-x)}\text{S}_2$  QDs for H<sub>2</sub> production. The pure ZnS QDs exhibits no photocatalytic activity for H<sub>2</sub> generation under visible light irradiation, which could be assigned to its wide bandgap (3.55 eV). After introducing the AgInS<sub>2</sub> component, which resulted in significantly increased H<sub>2</sub> production rate, indicating a synergistic interaction between the two components for the enhanced photocatalytic activities. The H<sub>2</sub> evolution activities increased remarkably and then decreased gradually with increasing x values, and the highest activity with a H<sub>2</sub> evolution rate of 276  $\text{mmol h}^{-1} \text{g}^{-1}$  was observed by using  $(\text{AgIn})_{0.5}\text{ZnS}_2$  QDs as the photosensitizer. The photocatalytic performance increased remarkably when x was increased from 0 to 0.5, which could be attributed to the increased absorption in the visible-light range.

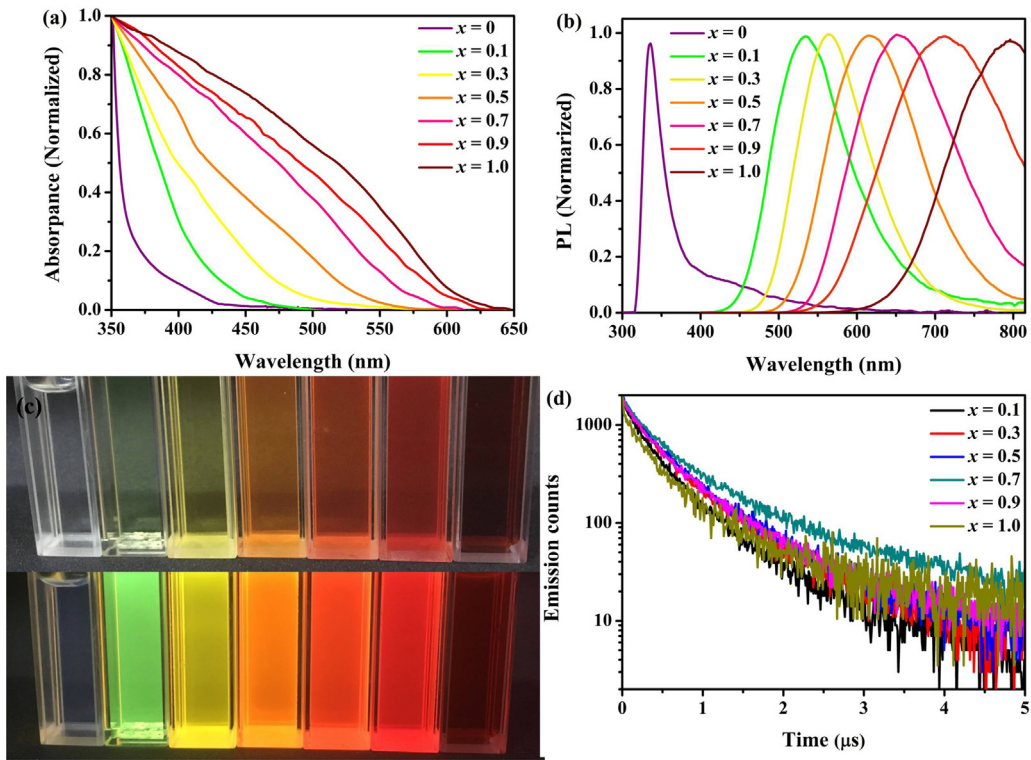


**Fig. 5.** (a,b) Absorption and emission spectra of ZnS, AgInS<sub>2</sub> and (AgIn)<sub>x</sub>Zn<sub>2(1-x)</sub>S<sub>2</sub> QDs in CH<sub>2</sub>Cl<sub>2</sub> solution, PL spectra was obtained by excitation at 350 nm (ZnS at 280 nm). (c) Photograph of ZnS, (AgIn)<sub>x</sub>Zn<sub>2(1-x)</sub>S<sub>2</sub> and AgInS<sub>2</sub> QDs without or under 365 nm UV light excitation in CH<sub>2</sub>Cl<sub>2</sub> (5 mg ml<sup>-1</sup>), from left to right: ZnS, (AgIn)<sub>x</sub>Zn<sub>2(1-x)</sub>S<sub>2</sub> QDs with x value of 0.1, 0.3, 0.5, 0.7, 0.9 and AgInS<sub>2</sub>. (d) Time-resolved PL spectra of (AgIn)<sub>x</sub>Zn<sub>2(1-x)</sub>S<sub>2</sub> QDs in CH<sub>2</sub>Cl<sub>2</sub> solution obtained by excitation at 465 nm ((AgIn)<sub>0.1</sub>Zn<sub>1.8</sub>S<sub>2</sub> at 345 nm).

When x exceeded 0.5, the photocatalytic activities decreased gradually with the increasing amount of AgInS<sub>2</sub>. The decreased in photocatalytic activities of (AgIn)<sub>x</sub>Zn<sub>2(1-x)</sub>S<sub>2</sub> QDs photosensitizers with a relatively larger amounts of AgInS<sub>2</sub> is likely due to the lower CB level [44]. That is, the CB of (AgIn)<sub>x</sub>Zn<sub>2(1-x)</sub>S<sub>2</sub> QDs became lower with increasing x values, and thus reducing the driving force for electron transfer from the excited (AgIn)<sub>x</sub>Zn<sub>2(1-x)</sub>S<sub>2</sub> QDs to the [Co(bpy)<sub>3</sub>]<sup>2+</sup> catalyst. As shown in Fig. 6b, the CB edge potential becomes more negative with increasing ZnS content (ie., decreasing x value) in the (AgIn)<sub>x</sub>Zn<sub>2(1-x)</sub>S<sub>2</sub> QDs, indicating that the ZnS-dominant QDs has strong reduction power ( $\Delta G_1 > \Delta G_2 > \Delta G_3$ ) for H<sub>2</sub> evolution reaction than the AgInS<sub>2</sub>-dominant QDs. However, the ZnS-dominant QDs have wider bandgaps than those of AgInS<sub>2</sub>-dominant QDs ( $E_{bg1} > E_{bg2} > E_{bg3}$ ), which is not desirable to use visible light as the energy source for the photocatalytic H<sub>2</sub> production reaction. This phenomenon could be assigned to a balance between the benefit of the stronger absorption in the visible-light range at high AgInS<sub>2</sub> contents with the need of ZnS to increase the driving force for charge carrier separation. Therefore, the balance between the light absorption capacity and the driving force in the (AgIn)<sub>0.5</sub>ZnS<sub>2</sub> QDs probably leads to the highest efficiency of visible light driven H<sub>2</sub> generation. Besides, the highest photocatalytic activity of (AgIn)<sub>0.5</sub>ZnS<sub>2</sub> QDs was also supported by the the emission quenching analysis, as discussed later. Notably, the turnover number (TON = TON = 2n(H<sub>2</sub>)/n(QDs)) values of (AgIn)<sub>x</sub>Zn<sub>2(1-x)</sub>S<sub>2</sub> QDs with x value of 0.1, 0.3, 0.5, 0.7 and 0.9, were observed to be 321, 908, 1268, 648 and 83, respectively. Previous studies have shown that both [Ir(ppy)<sub>2</sub>(bpy)]<sup>+</sup> and [Ru(bpy)<sub>3</sub>]<sup>2+</sup> were effective molecular photosensitizers for H<sub>2</sub> production with [Co(bpy)<sub>3</sub>]<sup>2+</sup> catalyst [49]. For comparison purposed, [Ir(ppy)<sub>2</sub>(bpy)]<sup>+</sup> and [Ru(bpy)<sub>3</sub>]<sup>2+</sup> were prepared and used as references under the same conditions. The results showed that the TON values with respect to the Ir(III) and Ru(II) photosen-

sitzers over 12 h of visible light irradiation were found to be 241 and 167, respectively. It is clear from our results that these (AgIn)<sub>x</sub>Zn<sub>2(1-x)</sub>S<sub>2</sub> (x = 0.1, 0.3, 0.5 and 0.7) QDs are considerably more efficient than commonly-used molecular photosensitzers, and the TON with respect to (AgIn)<sub>0.5</sub>ZnS<sub>2</sub> QDs is almost 5.26 and 7.59 times than [Ir(ppy)<sub>2</sub>bpy]<sup>+</sup> and [Ru(ppy)<sub>3</sub>]<sup>2+</sup> photosensitzers, respectively. These results indicate that the (AgIn)<sub>x</sub>Zn<sub>2(1-x)</sub>S<sub>2</sub> QDs could be an attractive alternative material to replace those metal complex photosensitzers for solar H<sub>2</sub> generation.

As shown in Fig. 7a, the H<sub>2</sub> evolution rate was found to depend on the concentration of (AgIn)<sub>x</sub>Zn<sub>2(1-x)</sub>S<sub>2</sub> QDs. When the concentration of (AgIn)<sub>0.5</sub>ZnS<sub>2</sub> QDs was increased to 20 from 1 μM, the mole of H<sub>2</sub> was increased to 834 from 121 μmol after 12 h of visible light irradiation. However, the TON with respect to (AgIn)<sub>0.5</sub>ZnS<sub>2</sub> is also lowering from 2420 to 417 when the concentration of (AgIn)<sub>0.5</sub>ZnS<sub>2</sub> QDs changes from 1 to 20 μM. The amounts of H<sub>2</sub> gas evolved from photocatalytic systems does not increase linearly with the (AgIn)<sub>x</sub>Zn<sub>2(1-x)</sub>S<sub>2</sub> QDs concentration, which could be assigned to the limiting concentration of [Co(bpy)<sub>3</sub>]<sup>2+</sup> catalyst. To determinate the apparent quantum yield (AQY) of photocatalytic H<sub>2</sub> production system, we used monochromatized light ( $\lambda = 450$  nm) introduced by a blue LED into the reaction vessel. For a typical H<sub>2</sub> production system containing 50 μM (AgIn)<sub>0.5</sub>ZnS<sub>2</sub>, 1 mM [Co(bpy)<sub>3</sub>]<sup>2+</sup> catalyst and 0.1 M H<sub>2</sub>A, the initial incident photons to H<sub>2</sub> yield was found to be 8.2% within a 2 h of irradiation.

When irradiation time was prolonged to 24 h, the H<sub>2</sub> evolution rate in (AgIn)<sub>0.5</sub>ZnS<sub>2</sub>–[Co(bpy)<sub>3</sub>]<sup>2+</sup>–H<sub>2</sub>A system is negligible. As there is a large amount of H<sub>2</sub>A existed in the photocatalytic system, the deactivation of H<sub>2</sub> evolution system should be caused by the consumption of (AgIn)<sub>0.5</sub>ZnS<sub>2</sub> QDs or/and [Co(bpy)<sub>3</sub>]<sup>2+</sup>. To reveal the reason for this deactivation, the same quantity of fresh (AgIn)<sub>0.5</sub>ZnS<sub>2</sub> QDs was added into the reaction system after 24 h irradiation. As shown in Fig. 7b, the photocatalytic system with

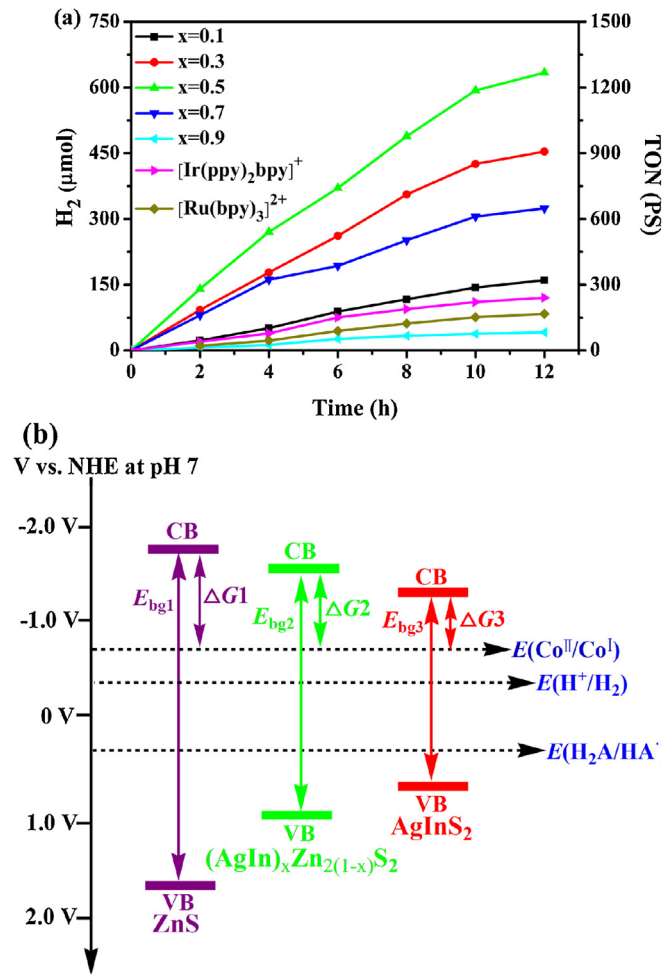


**Fig. 6.** (a) Photoinduced H<sub>2</sub> production traces with different (AgIn)<sub>x</sub>Zn<sub>2(1-x)</sub>S<sub>2</sub> QDs in 6:3:1 toluene-ethanol-water solution containing 10 μM (AgIn)<sub>x</sub>Zn<sub>2(1-x)</sub>S<sub>2</sub>, 1 mM [Co(bpy)<sub>3</sub>]<sup>2+</sup> and 0.1 M H<sub>2</sub>A under visible light irradiation ( $\lambda > 420$  nm); (b) conduction and valance band potentials of ZnS, AgInS<sub>2</sub> and (AgIn)<sub>x</sub>Zn<sub>2(1-x)</sub>S<sub>2</sub> QDs.

re-addition of [Co(bpy)<sub>3</sub>]<sup>2+</sup> showed an almost totally recovered activity for H<sub>2</sub> production under the same reaction conditions. If the same quantity of fresh (AgIn)<sub>0.5</sub>Zn<sub>2</sub>S<sub>2</sub> QDs was re-added to the inactive reaction solution following 12 h of visible light irradiation, H<sub>2</sub> did not resume. These results confirm both that the deactivation of photocatalytic H<sub>2</sub> evolution system can be attributed to the decomposition of the [Co(bpy)<sub>3</sub>]<sup>2+</sup> catalyst and also that the (AgIn)<sub>0.5</sub>Zn<sub>2</sub>S<sub>2</sub> QDs has sufficient photostability for solar H<sub>2</sub> generation. To further prove this hypothesis, the decomposition products extracted from the reaction solution of (AgIn)<sub>0.5</sub>Zn<sub>2</sub>S<sub>2</sub>-[Co(bpy)<sub>3</sub>]<sup>2+</sup>-H<sub>2</sub>A system were analyzed by gas chromatography-mass spectrometry (GC-MS) after the H<sub>2</sub> production leveled off. The GC-MS analysis clearly showed the 2,2'-bipyridine ligand dissociated from [Co(bpy)<sub>3</sub>]<sup>2+</sup> (Fig. S8), indicating that the decreasing H<sub>2</sub> production activity could be attributed to the photodecomposition of [Co(bpy)<sub>3</sub>]<sup>2+</sup> catalyst. Further studies are currently ongoing in our laboratory to develop long-term stable catalysts to match (AgIn)<sub>x</sub>Zn<sub>2(1-x)</sub>S<sub>2</sub> QDs for highly-efficient H<sub>2</sub> production system.

### 3.3. Reaction mechanisms for H<sub>2</sub> production

The conduction band of (AgIn)<sub>x</sub>Zn<sub>2(1-x)</sub>S<sub>2</sub> QDs ranged from  $-1.80$  ( $x=0$ ) to  $-1.08$  ( $x=1$ ) V (vs. NHE) [50,51], which are all more negative than the redox potential of the Co<sup>II</sup>/Co<sup>I</sup> couple ( $-0.95$  V vs. NHE) [52], thus providing the thermodynamic driving force

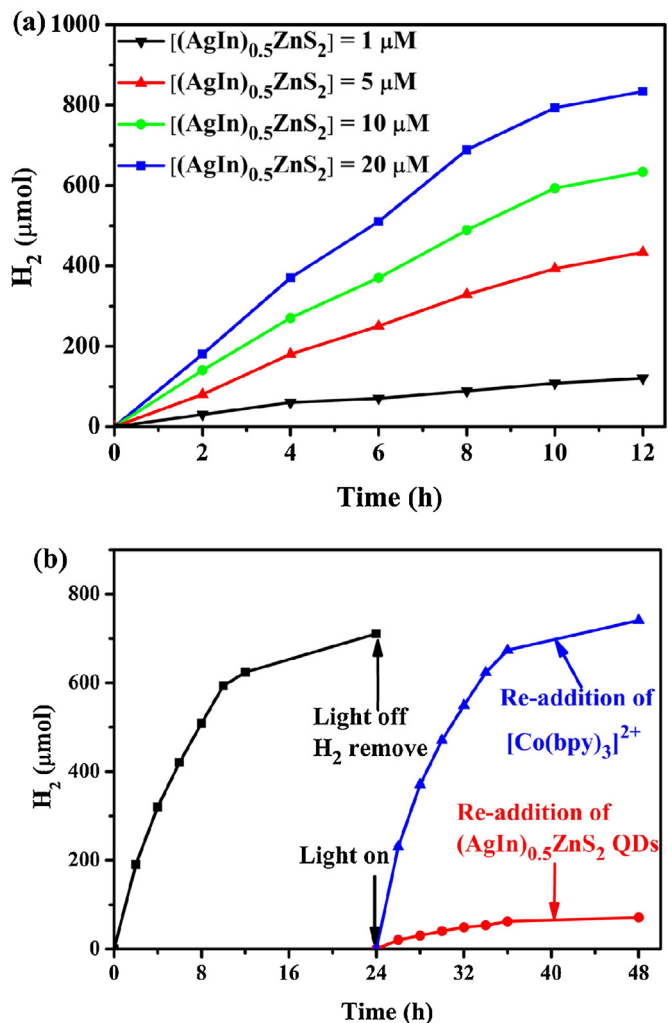


**Fig. 7.** (a) Photoinduced H<sub>2</sub> production traces with different initial concentrations of (AgIn)<sub>0.5</sub>Zn<sub>2</sub>S<sub>2</sub> QDs in 6:3:1 toluene-ethanol-water solution containing 1–20 μM (AgIn)<sub>0.5</sub>Zn<sub>2</sub>S<sub>2</sub>, 1 mM [Co(bpy)<sub>3</sub>]<sup>2+</sup> and 0.1 M H<sub>2</sub>A under visible light irradiation ( $\lambda > 420$  nm); (b) Stability test for (AgIn)<sub>0.5</sub>Zn<sub>2</sub>-[Co(bpy)<sub>3</sub>]<sup>2+</sup>-H<sub>2</sub>A photocatalytic H<sub>2</sub> evolution system in 6:3:1 toluene-ethanol-water solution containing 10 μM (AgIn)<sub>0.5</sub>Zn<sub>2</sub> QDs, 1 mM [Co(bpy)<sub>3</sub>]<sup>2+</sup> and 0.1 M H<sub>2</sub>A under visible light irradiation ( $\lambda > 420$  nm), activity is recovered upon re-addition of [Co(bpy)<sub>3</sub>]<sup>2+</sup> catalyst, but not upon re-addition of (AgIn)<sub>0.5</sub>Zn<sub>2</sub> QDs.

for efficient electron transfer from excited (AgIn)<sub>x</sub>Zn<sub>2(1-x)</sub>S<sub>2</sub> QDs to [Co(bpy)<sub>3</sub>]<sup>2+</sup> catalyst through an oxidative quenching pathway. On the other hand, the (AgIn)<sub>x</sub>Zn<sub>2(1-x)</sub>S<sub>2</sub> QDs have valance band ranging from  $+1.75$  ( $x=0$ ) to  $+0.72$  ( $x=1$ ) V (vs. NHE), which are more positive than the oxidation potential of H<sub>2</sub>A ( $+0.36$  V vs. NHE) [36], indicating that reductive quenching pathway for the electron-transfer quenching process between excited (AgIn)<sub>x</sub>Zn<sub>2(1-x)</sub>S<sub>2</sub> QDs and H<sub>2</sub>A is also feasible thermodynamically. In order to prove these analyses as described above, quenching experiments were conducted in 2:1 toluene-ethanol solution of the (AgIn)<sub>x</sub>Zn<sub>2(1-x)</sub>S<sub>2</sub> QDs by the addition of either [Co(bpy)<sub>3</sub>]<sup>2+</sup> as an electron acceptor or H<sub>2</sub>A as an electron donor. Representative emission quenching were shown in Fig. 8a and b, the emission spectrum of (AgIn)<sub>0.5</sub>Zn<sub>2</sub>S<sub>2</sub> QDs centered at 575 nm can be quenched efficiently by addition of either [Co(bpy)<sub>3</sub>]<sup>2+</sup> or H<sub>2</sub>A. Due to the small spectroscopic overlap of absorption of quenchers and emission of (AgIn)<sub>0.5</sub>Zn<sub>2</sub>S<sub>2</sub> QDs, the emission quenching observed in the present study is attributed to the photoinduced electron transfer between the excited QDs and quenchers. There are two different reaction pathways for the observed emission quenching: one is an oxidative

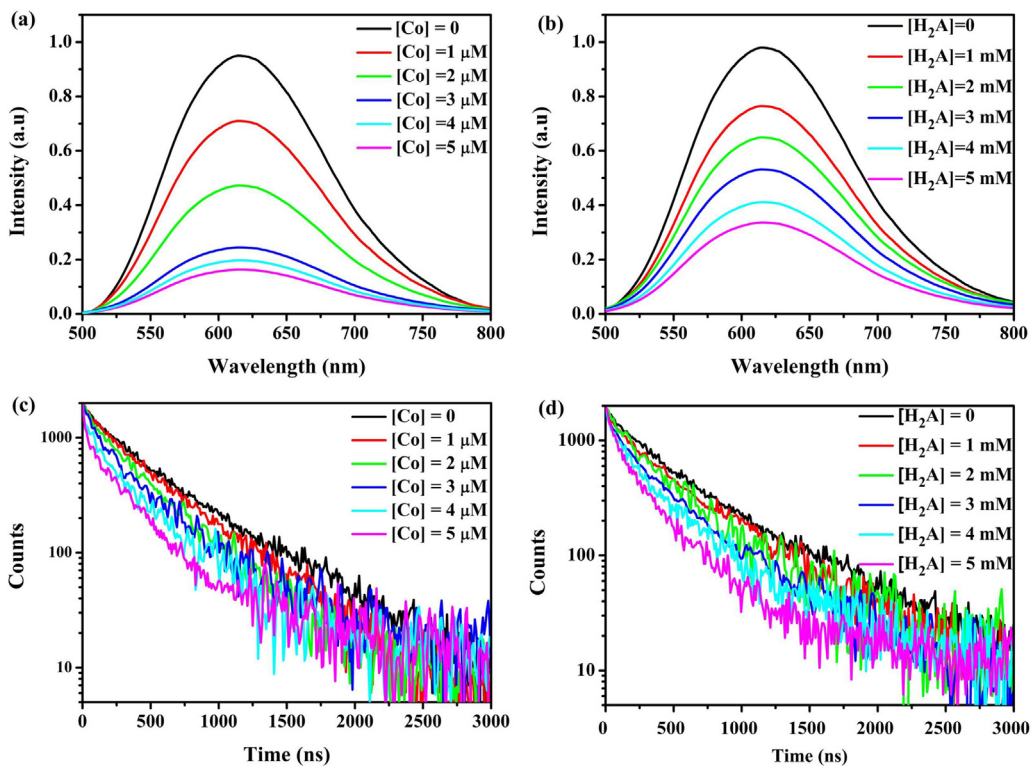
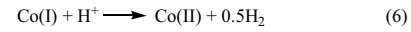
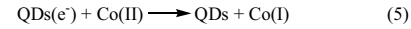
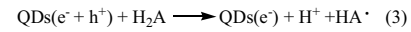
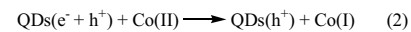
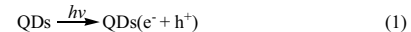


**Fig. 8.** Photoluminescence quenching of  $(\text{AgIn})_{0.5}\text{ZnS}_2$  QDs with progressive addition of  $[\text{Co}(\text{bpy})_3]^{2+}$  as an electron acceptor (a) or  $\text{H}_2\text{A}$  as an electron donor (b), the samples was excited at  $\lambda_{\text{ex}} = 350$  nm,  $[(\text{AgIn})_{0.5}\text{ZnS}_2] = 10 \mu\text{M}$ ; Time-resolved photoluminescence of colloidal  $(\text{AgIn})_{0.5}\text{ZnS}_2$  QDs upon addition of increasing amounts of  $[\text{Co}(\text{bpy})_3]^{2+}$  (c) or  $\text{H}_2\text{A}$  (d), the samples was excited at  $\lambda_{\text{ex}} = 465$  nm and monitored at  $\lambda_{\text{em}} = 575$  nm,  $[(\text{AgIn})_{0.5}\text{ZnS}_2] = 10 \mu\text{M}$ .

quenching pathway corresponds to electron transfer from the CB of  $(\text{AgIn})_x\text{Zn}_{2(1-x)}\text{S}_2$  QDs to  $[\text{Co}(\text{bpy})_3]^{2+}$  catalyst; while the other is a reductive quenching pathway corresponds to electron transfer from  $\text{H}_2\text{A}$  to the VB of  $(\text{AgIn})_x\text{Zn}_{2(1-x)}\text{S}_2$  QDs. For other  $(\text{AgIn})_x\text{Zn}_{2(1-x)}\text{S}_2$  QDs samples, their excited states were quenched dramatically upon the addition of increasing amounts of both  $[\text{Co}(\text{bpy})_3]^{2+}$  (Figs. S9–12) and  $\text{H}_2\text{A}$  (Figs. S13–S16) following Stern–Volmer plots (Figs. S17 and S18). The quenching constants  $K_q$  for each  $(\text{AgIn})_x\text{Zn}_{2(1-x)}\text{S}_2$  QDs samples with each of the quenchers are summarized in Table S1. Although  $\text{H}_2\text{A}$  is present of more than 100 times the concentration of  $[\text{Co}(\text{bpy})_3]^{2+}$ , the  $K_q$  values for oxidative quenching pathway were much higher than that of reductive quenching, indicating the  $\text{H}_2$  generation reaction is operating predominately through an oxidative quenching mechanism in the present study. In addition, the highest quenching constant was observed for  $(\text{AgIn})_{0.5}\text{ZnS}_2$  QDs with  $[\text{Co}(\text{bpy})_3]^{2+}$ , which was consistent with the highest photocatalytic performance of  $(\text{AgIn})_{0.5}\text{ZnS}_2$  QDs.

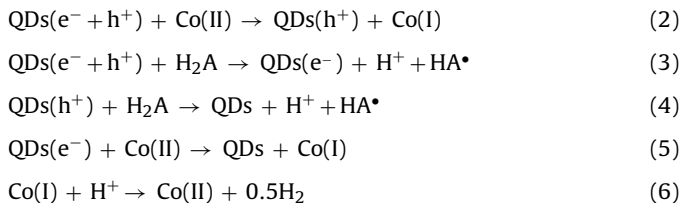
Furthermore, the excited lifetimes of  $(\text{AgIn})_x\text{Zn}_{2(1-x)}\text{S}_2$  QDs were analyzed to evaluate the electron-transfer kinetics between the excited QDs states and different quenchers. Fig. 8c shows the PL decay result of  $(\text{AgIn})_x\text{Zn}_{2(1-x)}\text{S}_2$  QDs with the addition of  $[\text{Co}(\text{bpy})_3]^{2+}$ . For the original  $(\text{AgIn})_x\text{Zn}_{2(1-x)}\text{S}_2$  QDs, the PL decay curve can be fitted with a nearly single-exponential function with a lifetime of 453 ns. After addition of 4, 8, 12, 16 and 20  $\mu\text{M}$   $[\text{Co}(\text{bpy})_3]^{2+}$ , the lifetime was decreased to 395, 297, 256, 172 and 141 ns, respectively. The lifetime decreased with the increasing concentration of  $[\text{Co}(\text{bpy})_3]^{2+}$ , corresponding to the efficient photoinduced electron transfer from excited  $(\text{AgIn})_x\text{Zn}_{2(1-x)}\text{S}_2$  QDs to  $[\text{Co}(\text{bpy})_3]^{2+}$ . On the other hand, hole transfer from the excited  $(\text{AgIn})_x\text{Zn}_{2(1-x)}\text{S}_2$  QDs to  $\text{H}_2\text{A}$  was also certified by the time-resolved PL decay curves shown in Fig. 8d. The results clearly reveal the charge carrier transfer between excited QDs and quenchers ( $[\text{Co}(\text{bpy})_3]^{2+}$  or  $\text{H}_2\text{A}$ ), which are well consistent with the trend of



**Scheme 1.** Proposed mechanism for photoinduced  $\text{H}_2$  production in  $(\text{AgIn})_x\text{Zn}_{2(1-x)}\text{S}_2\text{--}[\text{Co}(\text{bpy})_3]^{2+}\text{--H}_2\text{A}$  system.

the PL quenching results. Based on these observed measurements and observations, the proposed mechanism for photoinduced  $\text{H}_2$  production in  $(\text{AgIn})_x\text{Zn}_{2(1-x)}\text{S}_2\text{--}[\text{Co}(\text{bpy})_3]^{2+}\text{--H}_2\text{A}$  system was illustrated in Scheme 1. Under visible light irradiation, the electrons located on VB of  $(\text{AgIn})_x\text{Zn}_{2(1-x)}\text{S}_2$  QDs are excited to the CB, accompanied by the creation of holes in the VB (Eq. (1)). The excited QDs [QDs( $\text{e}^- + \text{h}^+$ )] is readily quenched by either  $[\text{Co}(\text{bpy})_3]^{2+}$  via an oxidative quenching pathway (Eq. (2)) or by  $\text{H}_2\text{A}$  via a reductive quenching pathway (Eq. (3)), the relative quenching rate constants (Table S1) suggest that the oxidative quenching with  $[\text{Co}(\text{bpy})_3]^{2+}$  dominates. During the oxidative quenching process, the photo-generated electrons were transferred to  $[\text{Co}(\text{bpy})_3]^{2+}$  catalyst, resulted in the formation of QDs( $\text{h}^+$ ) and Co(I) species. The oxidative QDs species with high oxidation potential was then reduced by  $\text{H}_2\text{A}$  to generate the ground-state QDs (Eq. (4)). On the other hand, the reduced QDs( $\text{e}^-$ ) resulted from the reductive quenching process can transfer an electron to  $[\text{Co}(\text{bpy})_3]^{2+}$  catalyst, forming the ground-state QDs photosensitizer and Co(I) complex (Eq. (5)). The Co(I) complex was proposed to be the most key intermediate [53], which absorbs protons and reduces them to evolve  $\text{H}_2$  with regeneration of the Co(II) catalyst (Eq. (6)).





#### 4. Conclusion

In conclusion, bandgaps of  $(\text{AgIn})_x\text{Zn}_{2(1-x)}\text{S}_2$  QDs are successfully engineered by controlling their composition with the aim of developing highly-efficient photosensitizers with low toxicity for photocatalytic  $\text{H}_2$  generation. The bandgaps of  $(\text{AgIn})_x\text{Zn}_{2(1-x)}\text{S}_2$  QDs can directly affect their light absorption capacity and driving force for photocatalytic  $\text{H}_2$  generation reaction, and a balance between the light absorption capacity and the driving force in  $(\text{AgIn})_{0.5}\text{ZnS}_2$  QDs leads to the highest efficiency of visible light driven  $\text{H}_2$  generation. An AQY of 8.2% at 450 nm was obtained in the photocatalytic  $\text{H}_2$  system comprised of  $(\text{AgIn})_{0.5}\text{ZnS}_2$  QDs as the photosensitizer,  $[\text{Co}(\text{bpy})_3]^{2+}$  as the catalyst, and  $\text{H}_2\text{A}$  sacrificial electron donor. The TON of  $\text{H}_2$  production in the  $(\text{AgIn})_{0.5}\text{ZnS}_2\text{-}[\text{Co}(\text{bpy})_3]^{2+}\text{-H}_2\text{A}$  system reached 2420 based on  $(\text{AgIn})_x\text{Zn}_{2(1-x)}\text{S}_2$  QDs over 12 h of visible light irradiation, which is almost 5.26 and 7.59 times than those of well-known  $[\text{Ir}(\text{ppy})_2\text{bpy}]^+$  and  $[\text{Ru}(\text{ppy})_3]^{2+}$  photosensitizers, respectively. The loss of  $\text{H}_2$  evolution activity of this present system can be attributed to the photodecomposition of  $[\text{Co}(\text{bpy})_3]^{2+}$ , whereas the  $(\text{AgIn})_x\text{Zn}_{2(1-x)}\text{S}_2$  QDs display a photostability of more than 48 h, thereby offering a significant advantage over rapidly photodegrading molecular photosensitizers. We believe that these findings will open a new strategy for the design of bandgap-tunable and durable semiconductor quantum dots with low toxicity for solar-to- $\text{H}_2$  conversion.

#### Acknowledgements

We are grateful for financial support from the National Natural Science Foundation of China (No. 51502068), the Natural Science Foundation of Zhejiang Province (No. LQ16B030002), the Natural Science Foundation of Zhejiang Province for Distinguished Young Scholars (LR15E020001) and the National Basic Research Program of China (No. 2013CB632404).

#### Appendix A. Supplementary data

Supplementary data associated with this article can be found, in the online version, at <http://dx.doi.org/10.1016/j.apcatb.2016.11.024>.

#### References

- [1] N.S. Lewis, D.G. Nocera, Proc. Natl. Acad. Sci. U. S. A. 103 (2006) 15729–15735.
- [2] H.J. Li, Y. Zhou, W.G. Tu, J.H. Ye, Z.G. Zou, Adv. Funct. Mater. 25 (2015) 998–1013.
- [3] D.Y. Kim, K.K. Sakimoto, D.C. Hong, P.D. Yang, Angew. Chem. Int. Ed. 54 (54) (2015) 3259–3266.
- [4] Q.J. Xiang, B. Cheng, J.G. Yu, Angew. Chem. Int. Ed. 54 (2015) 11350–11366.
- [5] K. Chang, Z.W. Mei, T. Wang, Q. Kang, S.X. Ouyang, J.H. Ye, ACS Nano 8 (2014) 7078–7087.
- [6] Y.J. Yuan, H.W. Lu, Z.T. Yu, Z.G. Zou, ChemSusChem 6 (2015) 4113–4127.
- [7] R. Kuriki, H. Matsunaga, T. Nakashima, K. Wada, A. Yamakata, O. Ishitani, K. Maeda, J. Am. Chem. Soc. 138 (138) (2016) 5159–5170.
- [8] D. Hollmann, F. Gärtnner, R. Ludwig, E. Barsch, H. Junge, M. Blug, S. Hoch, M. Beller, A. Brückner, Angew. Chem. Int. Ed. 50 (2011) 10246–10250.
- [9] Z.J. Han, L.X. Shen, W.W. Brennessel, P.L. Holland, R. Eisenberg, J. Am. Chem. Soc. 135 (2013) 14659–14669.
- [10] W.K.C. Lo, C.E. Castillo, R. Gueret, J. Fortage, M. Rebarz, M. Sliwa, F. Thomas, C.J. McAdam, G.B. Jameson, D.A. McMorrin, J.D. Crowley, M.N. Collomb, A.G. Blackman, Inorg. Chem. 55 (2016) 4564–4581.
- [11] K. Zhang, J.K. Kim, M. Ma, S.Y. Yim, C.L. Lee, H. Shin, J.H. Park, Adv. Funct. Mater. 26 (2016) 4527–4534.
- [12] W.D. Kim, J.H. Kim, S. Lee, S. Lee, J.Y. Woo, K. Lee, W.S. Chae, S. Jeong, W.K. Bae, J.A. McGuire, J.H. Moon, M.S. Jeong, D.C. Lee, Chem. Mater. 28 (2016) 962–968.
- [13] M.A. Gross, A. Reynal, J.R. Durrant, E. Reisner, J. Am. Chem. Soc. 136 (2014) 356–366.
- [14] B.F. Disalle, S. Bernhard, J. Am. Chem. Soc. 133 (2011) 11819–11821.
- [15] D.R. Whang, K. Sakai, S.Y. Park, Angew. Chem. Int. Ed. 52 (2013) 11612–11615.
- [16] X.H. Wang, S. Goeb, Z.Q. Ji, N.A. Pogulaichenko, F.N. Castellano, Inorg. Chem. 50 (2011) 705–707.
- [17] Y.J. Yuan, J.R. Tu, H.W. Lu, Z.T. Yu, X.X. Fan, Z.G. Zou, Dalton Trans. 45 (2016) 1359–1363.
- [18] Z.J. Han, L.X. Shen, W.W. Brennessel, P.L. Holland, R. Eisenberg, J. Am. Chem. Soc. 135 (2013) 14659–14669.
- [19] T. Sakai, D. Mersch, E. Reisner, Angew. Chem. Int. Ed. 52 (2013) 12313–12316.
- [20] Y.J. Yuan, Z.J. Ye, H.W. Lu, B. Hu, Y.H. Li, D.Q. Chen, J.S. Zhong, Z.T. Yu, Z.G. Zou, ACS Catal. 6 (2016) 532–541.
- [21] Y.J. Yuan, J.R. Tu, Z.J. Ye, D.Q. Chen, B. Hu, Y.W. Huang, T.T. Chen, D.P. Cao, Z.T. Yu, Z.G. Zou, Appl. Catal. B: Environ. 188 (2016) 13–22.
- [22] A. Das, Z.J. Han, W.W. Brennessel, P.L. Holland, R. Eisenberg, ACS Catal. 5 (2015) 1397–1406.
- [23] M. Wang, K. Han, S. Zhang, L.C. Sun, Coord. Chem. Soc. 287 (2015) 1–14.
- [24] J. Huang, K.L. Mulfort, P.W. Du, L.X. Chen, J. Am. Chem. Soc. 134 (2012) 16472–16475.
- [25] B.C.M. Martindale, G.A.M. Hutton, C.A. Caputo, E. Reisner, J. Am. Chem. Soc. 137 (2015) 6018–6025.
- [26] M.B. Wilker, K.E. Shinopoulos, K.A. Brown, D.W. Mulder, P.W. King, G. Dukovic, J. Am. Chem. Soc. 136 (2014) 4316–4324.
- [27] J.J. Wang, Z.J. Li, X.B. Li, X.B. Fang, Q.Y. Meng, S. Yu, C.B. Li, J.X. Li, C.H. Tung, L.Z. Wu, ChemSusChem 7 (2014) 1468–1472.
- [28] S. Cao, C.J. Wang, X.J. Lv, Y. Chen, W.F. Fu, Appl. Catal. B Environ. 162 (2015) 381–391.
- [29] F. Wang, W.J. Liang, J.X. Jian, C.B. Li, B. Chen, C.H. Tung, L.Z. Wu, Angew. Chem. Int. Ed. 52 (2013) 8134–8138.
- [30] C.B. Li, Z.J. Li, S. Yu, G.X. Wang, F. Wang, Q.Y. Meng, B. Chen, K. Feng, C.H. Tung, L.Z. Wu, Energy. Environ. Sci. 6 (2013) 2597–2602.
- [31] J.X. Jian, C. Ye, X.Z. Wang, M. Wen, Z.J. Li, X.B. Li, B. Chen, C.H. Tung, L.Z. Wu, Energy Environ. Sci. 9 (2016) 2083–2089.
- [32] W.J. Liang, F. Wang, M. Wen, J.X. Jian, X.Z. Wang, B. Chen, C.H. Tung, L.Z. Wu, Chem. Eur. J. 21 (2015) 3187–3192.
- [33] K.A. Brown, S. Dayal, X. Ai, G. Rumbles, P.W. King, J. Am. Chem. Soc. 132 (2010) 9672–9680.
- [34] J.X. Jian, Q. Liu, Z.J. Li, F. Wang, X.B. Li, C.B. Li, B. Liu, Q.Y. Meng, B. Chen, K. Feng, C.H. Tung, L.Z. Wu, Nat. Commun. 4 (2013) 2695.
- [35] K. Han, M. Wang, S. Zhang, S.L. Wu, Y. Yang, L.C. Sun, Chem. Commun. 51 (2015) 7008–7011.
- [36] C. Gimbert-Suriñach, J. Albero, T. Stoll, J. Fortage, M.N. Collomb, A. Deronzier, E. Palomares, A. Llobet, J. Am. Chem. Soc. 136 (2014) 7655–7661.
- [37] Z.J. Han, F. Qiu, R. Eisenberg, P.L. Holland, T.D. Krauss, Science 338 (2012) 1321–1324.
- [38] Y.J. Yuan, Z.T. Yu, J.G. Cai, C. Zheng, W. Huang, Z.G. Zou, ChemSusChem 6 (2013) 1357–1365.
- [39] W.R. McNameara, Z.J. Han, P.J. Alperin, W.W. Brennessel, P.L. Holland, R. Eisenberg, J. Am. Chem. Soc. 133 (2011) 15368–15371.
- [40] T. Kameyama, T. Takahashi, T. Machida, Y. Kamiya, T. Yamamoto, S. Kuwabata, T. Torimoto, J. Phys. Chem. C 119 (2015) 24740–24749.
- [41] J.M. Buriak, P.V. Kamat, K.S. Schanze, Acs. Appl. Mater. Interfaces 6 (2014) 11815–11816.
- [42] Z.C. Xu, C.M. Shen, Y.L. Hou, Chem. Mater. 21 (2009) 1778–1780.
- [43] T. Torimoto, T. Adachi, K. Okazaki, M. Sakuraoka, T. Shibayama, B. Ohtani, A. Kudo, S. Kuwabata, J. Am. Chem. Soc. 129 (2007) 12388–12389.
- [44] I. Tsuji, H. Kato, H. Kobayashi, A. Kudo, J. Am. Chem. Soc. 126 (2004) 13406–13413.
- [45] X.S. Tang, K. Yu, Q.H. Xu, E.S.G. Choo, G.K.L. Goh, J.M. Xue, J. Mater. Chem. 21 (2011) 11239–11243.
- [46] I. Mora-Sero, L. Bertoluzzi, V. Gonzalez-Pedro, S. Gimenez, F. Fabregat-Santiago, K.W. Kemp, E.H. Sargent, J. Bisquert, Nat. Commun. 4 (2013) 2272.
- [47] A.N. Cao, Z. Liu, S.S. Chu, M.H. Wu, Z.M. Ye, Z.W. Cai, Y.L. Chang, S.F. Wang, Q.H. Gong, Y.F. Liu, Adv. Mater. 22 (2010) 103–106.
- [48] I. Robel, M. Kuno, P.V. Kamat, J. Am. Chem. Soc. 129 (2007) 4136–4137.
- [49] J.I. Goldsmith, W.R. Hudson, M.S. Lowry, T.H. Anderson, S. Bernhard, J. Am. Chem. Soc. 127 (2005) 7502–7510.
- [50] N. Zeug, J. Bucheler, H. Kisch, J. Am. Chem. Soc. 107 (1985) 1459–1465.
- [51] W.J. Zhang, D.Z. Li, Z.X. Chen, M. Sun, W.J. Li, Q. Lin, X.Z. Fu, Mater. Res. Bull. 46 (2011) 975–982.
- [52] Y.J. Yuan, Z.T. Yu, H.L. Gao, Z.G. Zou, C. Zheng, W. Huang, Chem. Eur. J. 19 (2013) 6340–6349.
- [53] C.V. Krishnan, Bruce S. Brunschwig, C. Creutz, N. Sutin, J. Am. Chem. Soc. 107 (107) (1985) 2005–2015.